

OccludeNet: A Causal Journey into Mixed-View Actor-Centric Action Recognition under Occlusions

Guanyu Zhou¹, Wenxuan Liu¹, *Member, IEEE*, Wenxin Huang¹, *Member, IEEE*, Xuemei Jia¹,
Xian Zhong¹, *Senior Member, IEEE*, Chia-Wen Lin², *Fellow, IEEE*

Abstract—The lack of occlusion data in common action recognition video datasets limits model robustness and hinders consistent performance gains. We build OCCLUDENET, a large-scale occluded video dataset including both real and synthetic occlusion scenes in different natural settings. OCCLUDENET includes dynamic occlusion, static occlusion, and multi-view interactive occlusion, addressing gaps in current datasets. Our analysis shows occlusion affects action classes differently: actions with low scene relevance and partial body visibility see larger drops in accuracy. To overcome the limits of existing occlusion-aware methods, we propose a structural causal model for occluded scenes and introduce the Causal Action Recognition (CAR) method, which uses backdoor adjustment and counterfactual reasoning. This approach strengthens key actor information and improves model robustness to occlusion. We hope the challenges of OCCLUDENET will encourage more study of causal links in occluded scenes and lead to a fresh look at class relations, ultimately leading to lasting performance improvements. Our code and data is available at: <https://github.com/The-Martyr/OccludeNet-Dataset>.

Index Terms—Action Recognition, Occlusion, Counterfactual Reasoning, Class Correlation Profiling.

I. INTRODUCTION

Action recognition is essential for understanding human behavior [1], [2] and has achieved strong results on closed-set benchmarks such as KINETICS [3], UCF101 [4], and HMDB51 [5]. However, these datasets textitimize ideal conditions by filtering out ambiguous samples, which limits their applicability in real-world scenarios where actors are often occluded.

Current occlusion video datasets lack multi-view perspectives and effective motion information. To improve the robust ability of action recognition under occlusion environment, a preliminary exploration has been conducted of K-400-O [6].

Manuscript received June 7, 2025. This work was supported in part by the National Natural Science Foundation of China under Grants 62271361 and 62301213, and in part by the Hubei Provincial Key Research and Development Program under Grant 2024BAB039. (Corresponding author: Xian Zhong.)

Guanyu Zhou and Xian Zhong are with the Sanya Science and Education Innovation Park, Wuhan University of Technology, Sanya 572025, China, and the Hubei Key Laboratory of Transportation Internet of Things, Wuhan University of Technology, Wuhan 430070, China (e-mail: guanyuzhou.ai@gmail.com; zhongx@whut.edu.cn).

Wenxuan Liu is with the State Key Laboratory for Multimedia Info Processing, Peking University, Beijing 100871, China (e-mail: lwxfight@126.com).

Wenxin Huang is with the Hubei Key Laboratory of Big Data Intelligent Analysis, Hubei University, Wuhan 430062, China (e-mail: wenxin-huang_wh@163.com).

Xuemei Jia is with the National Engineering Research Center for Multimedia Software, Wuhan University, Wuhan 430072, China (e-mail: jiaxuemei@whu.edu.cn).

Chia-Wen Lin is with the Department of Electrical Engineering, National Tsing Hua University, Hsinchu 30013, Taiwan (e-mail: cwlin@ee.nthu.edu.tw).

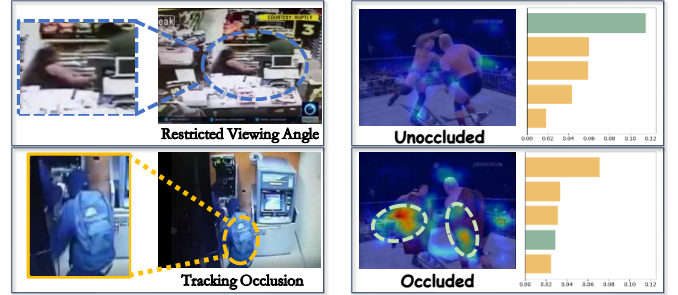


Fig. 1. Common real-world occlusions. Left: scenes exhibiting ambiguous occlusions. Right: Grad-CAM [7] visualizations of original and occluded KINETICS-400 [3] samples, illustrating how occlusions misdirect model attention and degrade performance. Green columns indicate the correct class.

However, it applies large-scale occlusions to the entire video frame under a single view. This strategy of adding occlusion akin to blind video reconstruction, neglecting the interrelations among scene elements and actions. *Diverse contextual elements* and *class correlations* under occlusions have not received the necessary attention.

By analyzing existing video occlusions (see Fig. 1), we present OCCLUDENET, a comprehensive occlusion video dataset that spans 424 action classes and incorporates diverse natural environment and occlusion types (see Fig. 2). It comprises dynamic tracking occlusions, static scene occlusions, and interactive occlusions: 1) OCCLUDENET-D: dynamic tracking occlusions involving moving actors; 2) OCCLUDENET-S: static scene occlusions by background elements; 3) OCCLUDENET-I: single-view interactive occlusions under changing lighting; 4) OCCLUDENET-M: multi-view interactive occlusions. By integrating both synthetic and real-world data, we enhance the dataset’s validity and scalability.

Existing de-occlusion models typically focus on minimizing the impact of occluded regions. However, the boundaries between occluders, backgrounds, and actors are often ambiguous. Traditional methods tend to rely on statistical correlations [8], thereby failing to capture the causal relations between occluders, backgrounds, visible actor parts, and predictions [9], [10].

We hypothesize that occlusion features serve as a confounder in the causal relation between actor attributes and model predictions [11]. To address this, we introduce a Causal Action Recognition (CAR) using a structural causal model that incorporates occlusion elements. Through counterfactual reasoning, our approach redirects the model’s focus to the causal influence of unoccluded actor features. We quantify this causal effect by calculating the difference between predictions

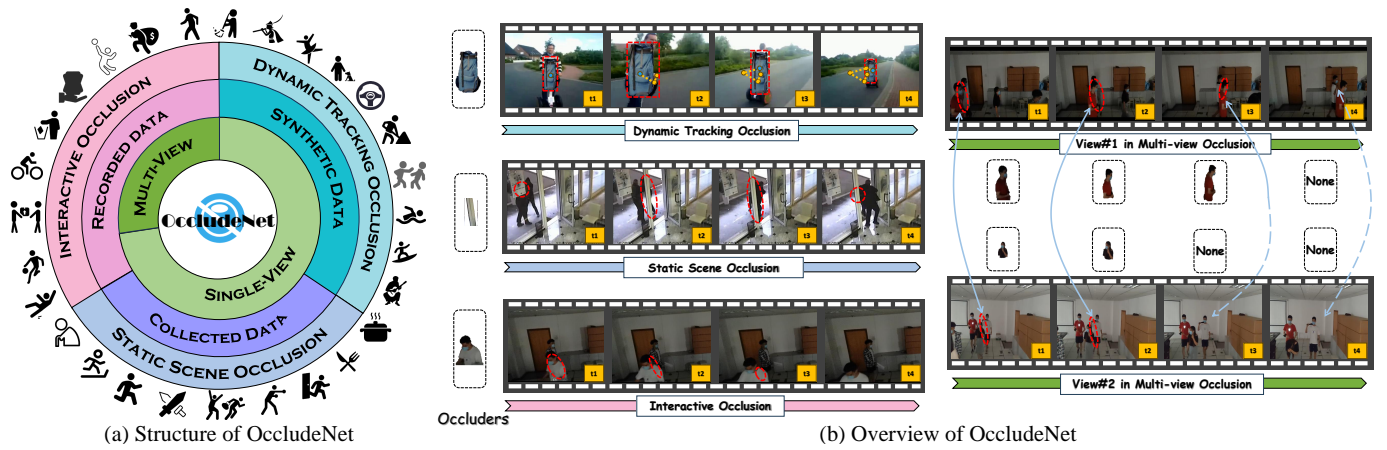


Fig. 2. **OCCLUDENET** dataset. (a) Hierarchical annotations: Coarse-to-fine labels of contextual elements from single- and multi-view videos covering three occlusion types, dynamic tracking, static scene, and interactive. Data are drawn from real recordings, curated collections, and synthetic sources. (b) Occlusion overview: Dynamic tracking occlusions feature an occluder following the actor (blue dot and orange trajectory); static scene occlusions use stationary occluders to partially block the actor; interactive occlusions arise from actor interactions (red dotted lines).

TABLE I

COMPARISON OF **OCCLUDENET** WITH EXISTING **OCCLUDED VIDEO ACTION RECOGNITION DATASETS**. SYN.: SYNTHESIZED; O-D: OCCUSION DURATION RATIO; “UNCROPPED” INDICATES AVAILABILITY OF FULL-FRAME CLIPS; “INTER-CLASS” DENOTES CLASS CORRELATION PROFILING.

Dataset	Type	#Clips	#Classes	#Occluders	O-D	View	Dynamics	Duration (s)	FPS	Uncropped	Inter-class
K-400-O [6]	Syn.	40,000	400	50	100%	Single-view	Geometric	12.0	24	×	×
UCF-101-O [6]	Syn.	3,783	101	50	100%	Single-view	Geometric	-	raw	×	×
UCF-19-Y-OCC [6]	Real	570	19	-	-	Single-view	-	4.0-5.0	23.98-30	×	×
OCCLUDENET-D	Syn.	233,769	400	2,788	0-100%	Single-view	Tracking	0.50-10.15	6-30	✓	✓
OCCLUDENET-S	Real	256	5	Varied	0-100%	Single-view	Static	8.0-10.0	25-30	✓	✓
OCCLUDENET-I	Real	345	7	Varied	0-100%	Single-view	Interactive	5.0-10.0	30	✓	✓
OCCLUDENET-M	Real	1,242	12	Varied	0-100%	Multi-view	Interactive	5.0-10.0	30	✓	✓

under occlusion and counterfactual predictions, interpreting the improvement in correct class probability as a positive treatment effect [11]. This method counteracts the accuracy loss due to occlusion by introducing an additional supervised signal that combines relative entropy loss with cross-entropy, thereby enhancing the model’s robustness to occlusions across various datasets.

In summary, our contributions are threefold:

- We construct an innovative dataset **OCCLUDENET**, designed specifically for occlusion-aware action recognition. It **uniquely** covers diverse occlusion scenarios, including *dynamic tracking* occlusions, *static scene* occlusions, and *multi-view interactive* occlusions. **OCCLUDENET** derives its strength from its comprehensive coverage of occlusion types, making it highly effective in addressing real-world problems with significant research value and practical applicability.
- We propose an insightful causal action recognition (CAR) framework that directs models to focus on unoccluded actor parts, enhancing robustness against occlusions.
- Our study reveals that occlusion strategies centered on actors influence action class recognition to varying degrees, highlighting the necessity of tailored approaches for addressing occlusions.

II. RELATED WORK

A. Action Recognition under Occlusion

Recent methods for action recognition under occlusion aim to improve model robustness. Early work trains classifiers on independently processed HOG blocks from multiple view-points [12] or handles blurred perspectives in multi-view settings [13]. Shi *et al.* [14] introduce a multi-stream graph convolutional network to manage diverse occlusion types. Chen *et al.* [15] show that pre-training on occluded skeleton sequences followed by k-means clustering enhances self-supervised skeleton-based action recognition. Liu *et al.* [16] propose a pseudo-occlusion strategy for real-world scenarios, and **OCCUSION SKELETON** [17] offers a valuable resource. Benchmark studies evaluate recognizer performance under occlusion [6]. Despite these advances, annotations remain labor-intensive and explicit causal modeling of occlusion effects is absent. There remains an urgent need for large-scale occluded datasets. Table I compares **OCCLUDENET** with existing occlusion datasets in terms of scale, occlusion dynamics, and sample characteristics.

B. Causal Inference in Computer Vision

Causal inference has gained traction in computer vision, with applications in autonomous driving [18] and robotics [11], [8], [19]. It has been integrated into explainable AI [20], fairness [21], [22], and reinforcement learning [23],

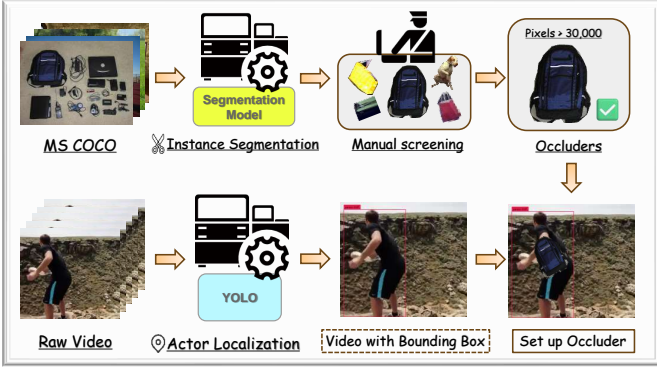


Fig. 3. **Construction process of OCCLUDENET-D.** For each frame, we detect the actor’s bounding box using YOLOv5 [28], center a random occluder on that box, and dynamically scale it to simulate tracking occlusion.

[24]. In compositional action recognition, counterfactual debiasing helps mitigate dataset biases [25], and in visual question answering, it reduces spurious correlations to yield more unbiased predictions [26], [27]. In this work, we leverage causal inference to enhance robustness in action recognition under occlusions, charting a new direction for vision research.

III. OCCLUDENET DATASET

We introduce OCCLUDENET, a **mixed-view** (multi-view and single-view) video dataset for action recognition, which includes three common types of occlusion (see Fig. 2(a)). This section provides an overview of the dataset’s construction, statistics, and features.

A. Dataset Construction

We construct a large-scale dataset of mixed-view occlusion videos captured under diverse natural lighting conditions, combining both synthetic and real-world data for enhanced validity and scalability. The dataset centers on key motion information and comprises four subsets (see Fig. 2(b)):

1) **OCCLUDENET-D (Dynamic Tracking Occlusion):** For dynamic tracking occlusion, we sample videos from KINETICS-400 [3] and introduce synthetic occluders as primary elements over actor bounding boxes to challenge recognition while preserving action identity. The construction process is illustrated in Fig. 3. We further evaluate the generalization capacity of synthetic data in V-A.

2) **OCCLUDENET-S (Static Scene Occlusion):** To focus on static occlusion, we select videos from UCF-CRIME [29] that prominently feature actors partially blocked by scene elements. These are then segmented into clips matching KINETICS-400 durations, providing realistic static-occlusion scenarios.

3) **OCCLUDENET-I (Single-View Interactive Occlusion):** We record continuous action sequences at 1920×1080 with a fixed RGB camera under varying lighting conditions. Participants with diverse body types and clothing styles wear masks for anonymity. Audio is retained for potential multi-modal analysis.

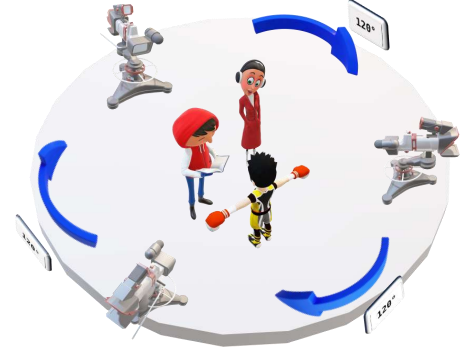


Fig. 4. **Recording setup of OCCLUDENET-M.** Three cameras, positioned 120° apart (blue arrows), simultaneously capture each action sequence from different directions.

4) **OCCLUDENET-M (Multi-View Interactive Occlusion):** For multi-view data, we employ synchronized RGB and near-infrared cameras at three angles spaced 120° apart to record the same action sequence. The setup and conditions mirror those of OCCLUDENET-I, ensuring uniform resolution, frame rate, and audio inclusion.

B. Quality Control

All videos undergo careful manual screening to ensure each clip accurately represents its action class with sufficient occlusion; approximately 4,000 samples were discarded due to blur or unrecognizability. We ensure diversity of actor appearance (body shape, clothing) and maintain occluder resolution above 30,000 pixels for visual clarity. All contributors (the authors) are professionally accountable for video quality. The entire dataset is uniformly annotated to facilitate efficient benchmarking across models.

C. Construction Details of OCCLUDENET-M

Fig. 4 presents the multi-view interactive occlusion setup. We record each action with three synchronized RGB and near-infrared camera pairs, positioned 120° apart around the actor. Occlusion conditions vary from single-view blockages to simultaneous multi-view occlusions, spanning different environments (indoor/outdoor), motion amplitudes (small gestures to large movements), and scales (near/far). Clips range from 5 s to over 10 s at 1920×1080 resolution, with audio retained for multimodal analysis.

D. Data Samples

1) **Video Samples:** Fig. 5 showcases example clips from OCCLUDENET, illustrating: a) *Occlusion Degree:* Light to heavy occlusion ratios. b) *Duration Ratio:* Fraction of the clip during which the actor is occluded. c) *Dynamics:* Static vs. moving occluders; single-view vs. multi-view interactions.

2) **Occluder Samples:** We select four common COCO objects [30], backpacks, handbags, suitcases, and dogs, to generate dynamic occlusions. Using a segmentation model, we extract their foreground masks. Each occluder retains its original filename and pixel-level annotation for traceability (see Fig. 6).



Fig. 5. **OCLUDET** samples under various occlusion conditions. Rows 1-3 show the same original video at low, medium, and high occlusion levels using the same occluder. Row 4 illustrates progressive partial occlusion over time. Row 5 depicts actors partially blocked by static scene elements, and Row 6 shows interactive occlusions between actors.



Fig. 6. **Occluder examples**. Rows 1-4 illustrate the four occluder types in **OCLUDET**: backpack, dog, suitcase, and handbag, ensuring a diverse range of occlusion patterns.

E. Additional Results and Visualizations

1) *Benchmarking and Analysis*: Fig. 7 plots Top-5 accuracy for seven models on **OCLUDET**. All models’ performance degrades as occlusion increases; CNN-based architectures suffer the largest drops, while transformer-based models show greater resilience.

2) *Class Correlation Profiling*: Figs. 8 and 9 analyze per-class accuracy drops. Actions with low scene relevance or partial body visibility (e.g., eating & drinking, head movements) exhibit the largest declines under occlusion. In contrast, background-dependent classes (e.g., water sports, racquet & bat sports) leverage context cues and are less impacted.

F. Diversity and Statistics of Occluded Dataset

1) **OCLUDET-D**: We randomly sample one-third of **KINETICS-400** clips and generate three occluded variants per

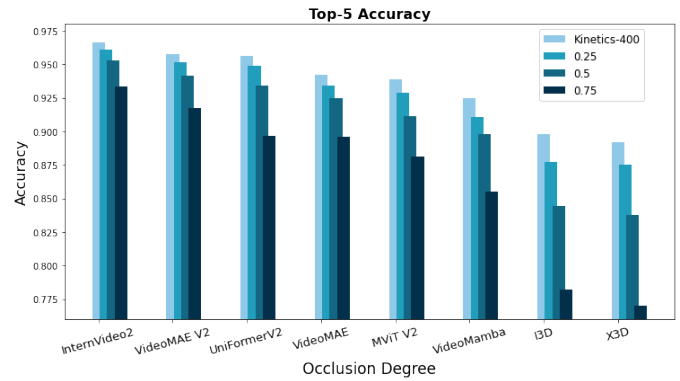


Fig. 7. **Top-5 accuracy drop on OCLUDET** at varying occlusion degrees. Results are shown for occlusion levels of 0.25, 0.50, and 0.75.

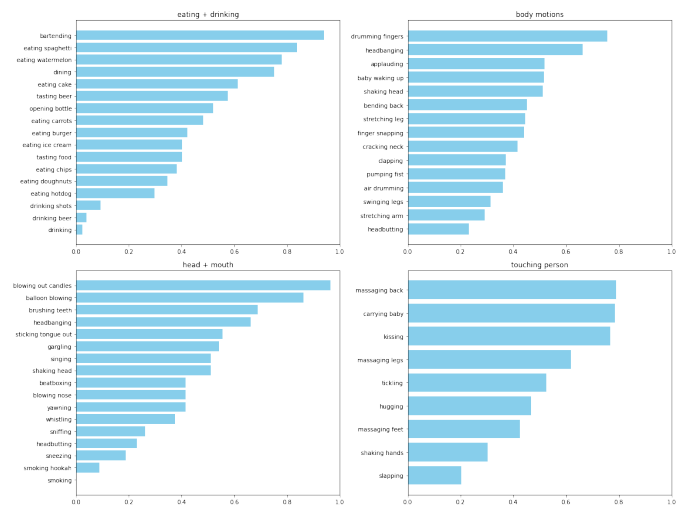


Fig. 8. **Subclasses of parent classes most affected by occlusion on OCLUDET**. The histogram (blue) highlights the relative accuracy drops for each subclass.

clip, with occluder scales at 0.25, 0.50, and 0.75 of the actor’s bounding box. Occluders, backpacks (153), handbags (118), suitcases (888), dogs (1,629), are drawn from **COCO** [30], yielding 233,769 clips across 400 classes.

2) **OCLUDET-S**: We curate 256 clips from **UCF-CRIME** [29] featuring static occlusions, trimmed to match **KINETICS-400** [3] durations. Classes include abuse (34), burglary (54), fighting (82), robbery (54), and stealing (32). Audio is preserved.

3) **OCLUDET-I**: Seven action classes, affix poster, armed, basketball dribble, basketball shot, bike ride, indoor run, walk, are recorded with masked participants of varied body shapes and attire. Occlusion modes, levels, and durations differ per clip. Splits: train 80%, val 5%, test 15%.

4) **OCLUDET-M**: Twelve classes, armed, basketball dribble, basketball shot, bike ride, distribute leaflets, fall, indoor run, outdoor run, steal, throw things, walk, wander, are captured from three views, each with unique occlusions. Splits: train 80%, val 5%, test 15%.

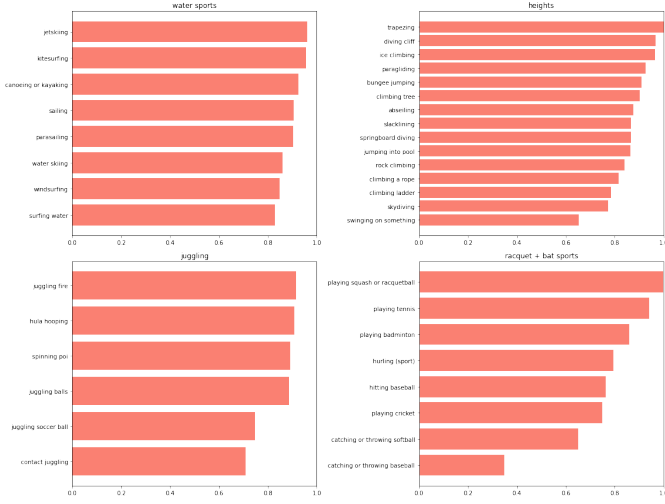


Fig. 9. Subclasses of parent classes least affected by occlusion on OCLUDEDNET. The histogram (red) highlights the relative accuracy changes for each subclass.

G. Dataset Characteristics Analysis

1) *Preliminary Analysis*: OCLUDEDNET covers object, scene, and view-variation occlusions with levels from light to heavy. It captures dynamic occlusion patterns, abrupt onset, gradual intensification, and intermittent, creating a challenging evaluation environment.

2) *Impact of Individual Occlusion Factors*: Fig. 10 defines three metrics: a) *Occlusion Degree*: Occluder size relative to actor’s bounding box. b) *Area Ratio*: Percentage of actor bounding box occluded. c) *Duration Ratio*: Fraction of clip time actor is occluded.

3) *Class Correlation Profiling*: Fig. 11 shows that classes with low background relevance or limited visibility (e.g., upper-body actions) experience the largest accuracy drops, underscoring the need for occlusion-aware modeling.

IV. CAUSAL ACTION RECOGNITION

We introduce the Causal Action Recognition (CAR) framework, shown in Fig. 12, which models interactions among actors, occlusions, and backgrounds via diverse contextual elements to improve action recognition. This section details CAR’s components: occlusion scene modeling (see Section IV-A), intervention strategies (see Section IV-B), and counterfactual reasoning (see Section IV-C).

A. Modeling Occluded Scenes

We represent occluded scenes with a structural causal model (SCM) as a directed acyclic graph, where nodes are variables and edges are causal links. The prediction P is given by

$$P = f(A, B, F, O, \epsilon_P), \quad (1)$$

where f : mapping function (e.g., neural network modules), A : actor features extracted from the visible body parts, B : background features capturing scene context, F : additional contextual features (e.g., motion cues), O : occlusion features

encoding the occluder’s appearance and location, ϵ_P : independent noise term. We further define

$$B = g(O, \epsilon_B), \quad F = h(O, \epsilon_F), \quad A = k(O, \epsilon_A), \quad (2)$$

so that each feature is influenced by occlusion O and its respective noise. This SCM captures how occlusion affects P , forming the basis of CAR’s robustness to occlusions.

B. Causal Intervention Strategies

To isolate the causal effect of A on P , we apply Pearl’s do-calculus [11], treating O as a confounder. We compute the interventional prediction

$$P(\text{do}(A = a)), \quad (3)$$

which reflects P when A is set to a , independent of O . We then use back-door adjustment to block O ’s influence:

$$P(P | \text{do}(A)) = \sum_o P(P | A, o)P(o). \quad (4)$$

Implementation relies on precise actor segmentation and tracking via Grounded-SAM [31], [32], Segment-and-Track-Anything [33], [34], and EfficientVit-SAM [35], enabling controlled manipulation of A .

C. Counterfactual Reasoning and Learning

Counterfactual reasoning compares original and intervened predictions to quantify A ’s causal effect:

$$P_{\text{effect}} = \mathbb{E}_{A \sim \tilde{A}} [P(A = \mathbf{A}, O = \mathbf{O}) - P(\text{do}(A = \mathbf{a}), O = \mathbf{O})], \quad (5)$$

where \tilde{A} is the manipulated feature distribution, \mathbf{A} is the observed actor state, \mathbf{a} is the counterfactual state. Denote logits for original and counterfactual predictions by p_i and c_i . The softmax probabilities are

$$P = \left(\frac{\exp(p_1)}{\sum_{j=1}^n \exp(p_j)}, \frac{\exp(p_2)}{\sum_{j=1}^n \exp(p_j)}, \dots, \frac{\exp(p_n)}{\sum_{j=1}^n \exp(p_j)} \right), \quad (6)$$

ensuring that P sums to 1 across all classes. The corrected prediction Y is derived from the difference between the logits:

$$Y = \left(\frac{\exp(p_i - c_i)}{\sum_{j=1}^n \exp(p_j - c_j)} \right)_{i=1}^n. \quad (7)$$

We combine cross-entropy and causal (Kullback-Leibler divergence) losses:

$$\mathcal{L} = - \sum_{i=1}^n P_i \log \hat{P}_i + \alpha \sum_{i=1}^n P_i \log \frac{P_i}{Y_i}, \quad (8)$$

where P_i and Y_i are defined as above (original and counterfactual softmax probabilities); \hat{P}_i is the one-hot ground-truth label for class i ; α is a balancing hyperparameter that weights the causal (KL) term relative to the cross-entropy term. This counterfactual supervision during fine-tuning enhances occlusion robustness without added inference cost.

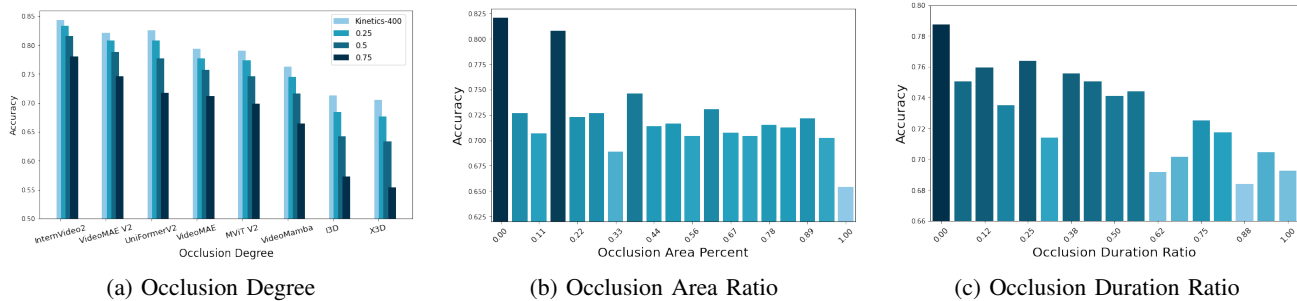


Fig. 10. **Impact of individual occlusion factors on recognition accuracy in OCCLUDENET.** (a) Occlusion degree: ratio of the occluder’s size to the actor bounding box; (b) occlusion area ratio: percentage of the actor bounding box that is occluded; (c) occlusion duration ratio: fraction of frames in which the actor is occluded.

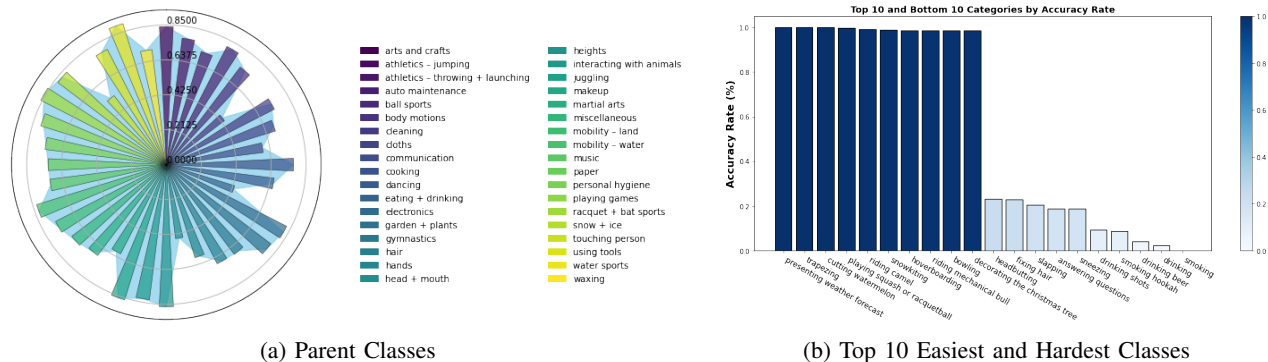


Fig. 11. **Class correlation analysis on OCCLUDENET.** (a) Overall accuracy for each parent class. (b) Top 10 classes with the highest and lowest accuracy, averaged across all models.

TABLE II

TOP-1 ACCURACY (%) OF VARIOUS MODELS ON OCCLUDED DATASETS. D-25, D-50, AND D-75 DENOTE OCCLUDENET-D OCCLUSION LEVELS (25%, 50%, 75%). K-O, O-S, O-I, AND O-M REFER TO K-400-O, OCCLUDENET-S, OCCLUDENET-I, AND OCCLUDENET-M, RESPECTIVELY. “K-400” INDICATES PERFORMANCE ON THE ORIGINAL KINETICS-400.

Method	Venue	Backbone	K-O	D-25	D-50	D-75	O-S	O-I	O-M	K-400
I3D [36]	CVPR’17	ResNet-50	33.6	68.48	64.26	57.26	15.09	10.19	9.86	71.28
X3D [37]	CVPR’20	ResNet-50	34.3	67.60	63.34	55.43	16.98	19.44	2.90	70.47
MViTv2 [38]	CVPR’22	Transformer	56.7	77.35	74.64	69.83	26.42	24.07	1.16	79.01
VideoMAE [39]	NeurIPS’22	Transformer	58.1	77.67	75.72	71.14	32.08	3.70	4.06	79.34
UniFormerv2 [40]	ICCV’23	Transformer	-	80.82	77.68	71.79	20.75	7.41	11.30	82.60
VideoMAEv2 [41]	CVPR’23	Transformer	-	80.81	78.85	74.66	7.55	2.78	17.39	82.15
VideoMamba [42]	ECCV’24	Mamba	-	74.54	71.68	66.43	22.96	22.53	10.55	76.28
InternVideo2 [43]	arXiv’24	Transformer	-	83.33	81.61	78.04	20.12	16.19	3.61	84.34

V. EXPERIMENTAL RESULTS

A. Benchmarking and Analysis

a) Experimental Setup: We evaluate eight state-of-the-art models on KINETICS-400 [3], K-400-O [6], and our OCCLUDENET test set. The models are InternVideo2 [43], VideoMamba [42], UniFormerv2 [40], VideoMAEv2 [41], VideoMAE [39], MVITv2 [38], X3D [37], and I3D [36]. We use the mmaction2 framework [44] and pretrained weights for all models except VideoMamba and InternVideo2. Table II summarizes Top-1 and Top-5 accuracies across datasets.

b) Influencing Factors Analysis: Across all models, accuracy steadily declines as occlusion degree increases (see Fig. 10(a)). CNN-based models (I3D, X3D) suffer the steepest drops. Similarly, Fig. 10(b) shows that larger occlusion area ratios, *i.e.*, greater occluder coverage of the actor’s bounding box, lead to further accuracy loss. Finally, longer occlusion

durations (see Fig. 10(c)) reduce recognition performance, since fewer visible frames remain.

c) Parent-Class Impact: We group actions by parent classes (*e.g.*, “Music” includes playing drums, trombone, violin) as in [3]. Fig. 11(a) shows that occlusion most severely affects body-motion, eating & drinking, head & mouth, and “touching persons” classes. These actions rely heavily on body parts occupying large frame areas with minimal background cues, making them vulnerable when occluded.

d) Class-Specific Characteristics: Fig. 11(b) details per-class accuracy changes on OCCLUDENET-D. Diet-related actions (eating burgers, watermelon), head-focused actions (brushing teeth, curling hair), hand-centric actions (nail clipping, clapping, sign language), and instrumental actions (playing flute, saxophone) show large drops, as models depend on actor features. In contrast, background-dependent actions

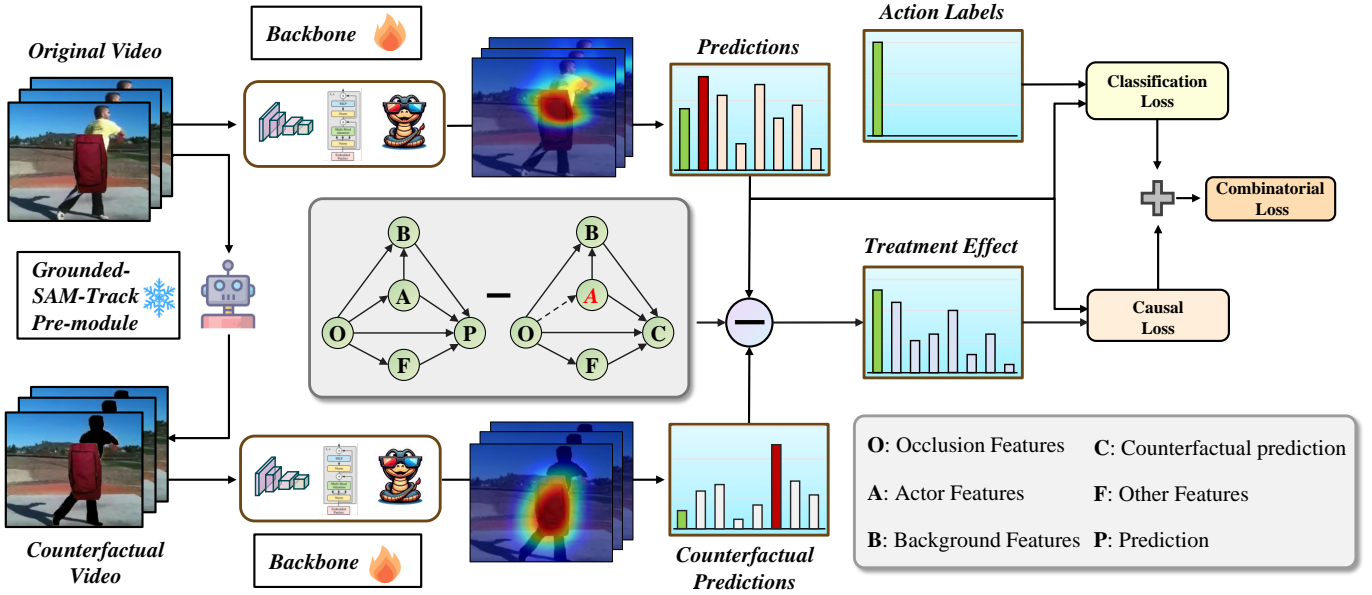


Fig. 12. **Pipeline of CAR.** A preprocessing module generates counterfactual samples that, alongside the original inputs, pass through a shared backbone to produce separate predictions. The discrepancy between these predictions provides a supervised signal via a custom loss, reducing bias from incorrect feature attributions.

TABLE III
ABLATION STUDY ON OCCLUSION DEGREE IN OCLUDENET.
UNOCCLUDED, SLIGHT, MODERATE, AND HEAVY DENOTE INCREASING
OCCLUSION LEVELS.

Metric	Unoccluded	Slight	Moderate	Heavy
Top-1 (%)	77.30	75.32	72.31	66.65
Top-5 (%)	93.00	91.89	89.87	85.69

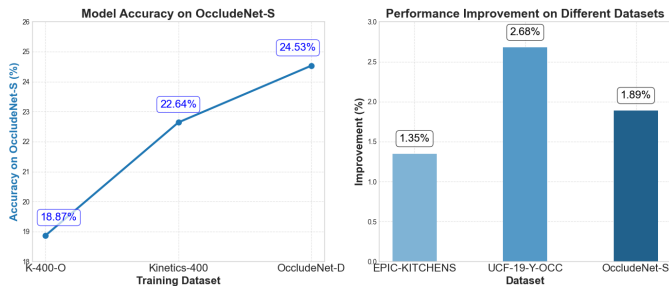


Fig. 13. **Generalization evaluation of OCLUDENET-D.** Left: A model trained on OCLUDENET-D achieves peak accuracy (24.53%) on real-world occluded data. Right: Incorporating OCLUDENET-D in training yields performance gains across multiple datasets.

(swimming, surfing, rock climbing) are less impacted, leveraging contextual cues.

e) *Generalization of Synthetic Data:* We perform an ablation using UniFormerv2 [40] (see Table III). Although synthetic occlusions reduce model accuracy, human observers still recognize the actions, underscoring the challenge.

Training on OCLUDENET-D and testing on real occluded data (see Fig. 13) shows that synthetic-trained models achieve higher accuracy across datasets, demonstrating improved robustness and generalization.

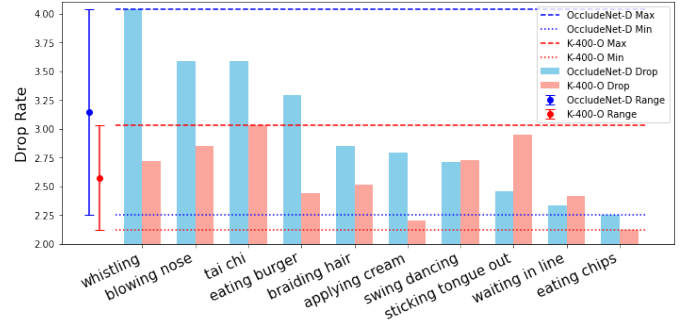


Fig. 14. **Impact of occlusion strategy on recognition accuracy.** For VideoMAE [39], MVITv2 [38], I3D [36], and X3D [37], OCLUDENET-D induces Top-1 accuracy drops at occlusion levels of 0.25, 0.50, and 0.75, compared to K-400-O. The ten classes with the largest drops on OCLUDENET-D were selected at random.

f) *Dataset Sustainability Discussion:* Fig. 14 compares inter-class accuracy variance on K-400-O versus OCLUDENET-D. Heavy, blind occlusions in K-400-O render recognition nearly impossible, even for humans. By contrast, OCLUDENET-D retains sufficient visual cues for human recognition, supporting sustainable accuracy improvements and robustness under occlusion.

B. Causal Action Recognition

To assess causal modeling, we compare CAR against background-modeling baselines (StillMix [9], FAME [10]). We fine-tune UniFormerv2-B/16 [40] (CLIP-400M+K710 pre-train) for 5 epochs on OCLUDENET. For OCLUDENET-S, we fine-tune X3D-S [37], UniFormerv2-B, and VideoMamba-M [42] for 5 and 10 epochs using both baseline and CAR losses.

TABLE IV
TOP-1 AND TOP-5 ACCURACY (%) OF ADVANCED METHODS ON OCCLUDED AND STANDARD DATASETS. D-25, D-50, D-75 DENOTE OCCLUDENET-D OCCLUSION LEVELS (25%, 50%, 75%). EPIC REFERS TO THE PREPROCESSED EPIC-KITCHENS CLIPS. STILLMIX [9] AND FAME [10] ARE NOT APPLICABLE TO K-400-O OR EPIC-KITCHENS.

Method	Backbone	D-25	D-50	D-75	KINETICS-400	K-400-O	Epic-Kitchens
StillMix [9]	Swin Transformer	55.35 / 79.59	53.72 / 78.55	51.63 / 76.27	57.63 / 81.21	-	-
FAME [10]	Swin Transformer	55.13 / 79.88	54.21 / 78.72	51.64 / 76.33	57.41 / 80.98	-	-
UniFormerv2 [40]	CNN + Transformer	88.37 / 97.69	87.16 / 97.25	85.13 / 96.50	88.31 / 97.71	57.75 / 77.47	35.81 / 79.05
UniFormerv2 + CAR	CNN + Transformer	88.63 / 97.77	87.61 / 97.74	85.50 / 96.66	88.98 / 97.99	57.75 / 77.80	37.16 / 81.76

TABLE V
TOP-1 ACCURACY (%) OF BASELINE vs. CAR-ENHANCED MODELS ON OCCLUDENET-S, OCCLUDENET-I, AND OCCLUDENET-M. S-5/-10: TRAINED FOR 5/10 EPOCHS ON OCCLUDENET-S; O-I/-M: OCCLUDENET-I/OCCLUDENET-M. "Δ" DENOTES IMPROVEMENT WITH CAR.

Method	S-5	S-10	O-I	O-M
X3D [37]	26.42	20.75	52.78	6.09
X3D + CAR	26.42	28.30	54.63	8.70
Δ	+0.00	+7.55	+1.85	+2.61
UniFormerv2 [40]	79.25	84.91	14.81	19.13
UniFormerv2 + CAR	81.13	86.78	15.74	23.77
Δ	+1.88	+1.87	+0.93	+4.64
VideoMamba [42]	26.25	33.64	22.53	32.46
VideoMamba + CAR	27.04	34.75	24.92	34.49
Δ	+0.79	+1.11	+2.39	+2.03

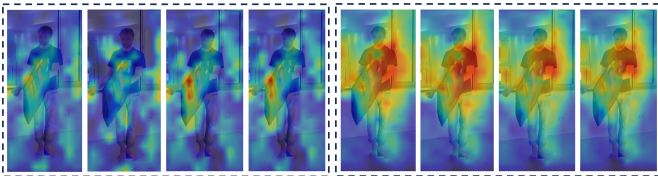


Fig. 15. **Grad-CAM class activation map comparison** [7]. Baseline (left) versus CAR (right) illustrates that CAR shifts attention from occluders to the actor’s action regions, improving focus on relevant features and boosting recognition accuracy.

a) *Results and Generalization:* Tables IV and V report accuracies on OCCLUDENET, KINETICS-400, K-400-O, and EPIC-KITCHENS [45]. CAR consistently outperforms baselines, mitigating occlusion-induced degradation.

Grad-CAM visualizations (see Fig. 15) confirm that CAR redirects attention from occluders and backgrounds to the actor’s key regions, even on unobstructed KINETICS-400 videos.

b) *Causal Inference Ablation.:* We vary the loss balance hyperparameter α (see Table VI) to evaluate its effect on robustness. Results indicate that an optimal α range significantly enhances performance under occlusion.

c) *Grad-CAM Visualization:* Fig. 16 shows Grad-CAM attention maps [7]. On OCCLUDENET dataset, CAR focuses strongly on unoccluded actor regions and key action cues, whereas the baseline model often attends to occluders. Even on the unconstrained KINETICS-400 videos, CAR produces more concentrated attention on the actor’s movements. These results confirm that CAR not only bolsters occlusion robustness but also refines the model’s attention distribution.

TABLE VI
ABLATION ON α FOR CAR’S TOP-1/TOP-5 ACCURACY (%) ON OCCLUDENET-D.

α	D-25	D-50	D-75
0	88.37 / 97.69	87.16 / 97.25	85.13 / 96.50
0.5	88.18 / 97.72	87.36 / 97.46	85.23 / 96.56
1.0	88.63 / 97.77	87.61 / 97.74	85.50 / 96.66
2.0	88.24 / 97.75	73.02 / 93.65	85.19 / 96.57

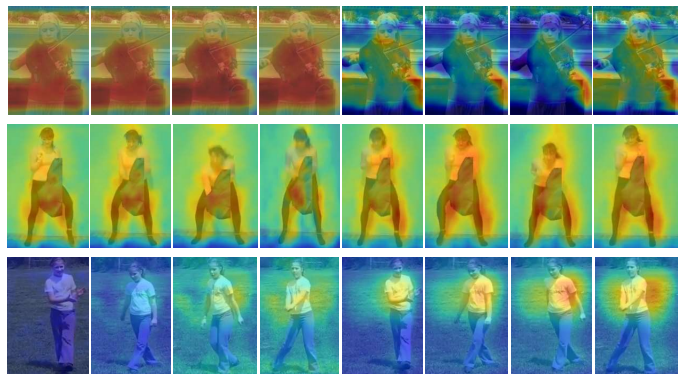


Fig. 16. **Comparison of class activation maps.** Grad-CAM [7] visualizations for the baseline (left) and CAR (right) models. CAR redirects attention from occluders to the actor’s action regions and, even on non-occluded KINETICS-400 samples, produces more focused attention on the actor’s movements.

d) *Comparison with Actor-Mask Training.:* We have also tried to use actor masks directly for auxiliary training, but due to data diversity, it often lacks continuity. Retaining only the body may fail to convey the action class, while the background and occluders, no longer featuring the actor’s action, tend to be more continuous. This reflects the necessity of our causal modeling. The specific experimental data are in tab VII.

VI. CONCLUSION

We introduce OCCLUDENET, a large-scale video dataset simulating dynamic tracking, static scene, and multi-view interactive occlusions. Our analysis reveals that occlusion strategies impact action classes unevenly, with the greatest accuracy drops for actions featuring low scene relevance and partial body visibility. To mitigate this, we propose the CAR framework, which models occluded scenes via a structural causal model and leverages back-door adjustment and counterfactual reasoning to refocus on unoccluded actor features, significantly improving robustness.

Applications: 1) *Security and surveillance:* Surveillance footage often suffers from limited viewpoints and intentional

TABLE VII
COMPARISON WITH ACTOR-MASK TRAINING. CAR OUTPERFORMS
DIRECT ACTOR-MASK SUPERVISION ACROSS OCCLUSION LEVELS.

Method	D-25	D-50	D-75
Actor mask	88.21 / 97.65	87.10 / 97.21	85.13 / 96.46
CAR (ours)	88.63 / 97.77	87.61 / 97.74	85.50 / 96.66

obstructions. OCCLUDENET provides realistic occlusion scenarios to train and evaluate models for more reliable monitoring. 2) *Virtual scenes*: In short-form and live videos, virtual occlusions such as subtitles, stickers, and tracking effects abound. Our dataset can simulate these artifacts, guiding methods to handle them effectively. 3) *Occlusion localization*: By exposing models to varied occlusions, 4) OCCLUDENET enables future work on pinpointing occluded regions within frames, advancing spatial understanding. 5) *Multi-modal analysis*: All clips include audio, supporting integrated audio-visual learning and reflecting the trend toward multi-modal video understanding.

REFERENCES

- [1] S. Herath, M. T. Harandi, and F. Porikli, "Going deeper into action recognition: A survey," *Image Vis. Comput.*, vol. 60, pp. 4–21, 2017.
- [2] Y. Kong and Y. Fu, "Human action recognition and prediction: A survey," *Int. J. Comput. Vis.*, vol. 130, no. 5, pp. 1366–1401, 2022.
- [3] W. Kay, J. Carreira, K. Simonyan, B. Zhang, C. Hillier, S. Vijayanarasimhan, F. Viola, T. Green, T. Back, P. Natsev, M. Suleyman, and A. Zisserman, "The kinetics human action video dataset," *arXiv preprint arXiv:1705.06950*, 2017.
- [4] K. Soomro, A. R. Zamir, and M. Shah, "UCF101: A dataset of 101 human actions classes from videos in the wild," *arXiv preprint arXiv:1212.0402*, 2012.
- [5] H. Kuehne, H. Jhuang, E. Garrote, T. A. Poggio, and T. Serre, "HMDB: A large video database for human motion recognition," in *Proc. IEEE/CVF Int. Conf. Comput. Vis.*, 2011, pp. 2556–2563.
- [6] S. Grover, V. Vineet, and Y. S. Rawat, "Revealing the unseen: Benchmarking video action recognition under occlusion," in *Adv. Neural Inf. Process. Syst.*, 2023.
- [7] R. R. Selvaraju, M. Cogswell, A. Das, R. Vedantam, D. Parikh, and D. Batra, "Grad-cam: Visual explanations from deep networks via gradient-based localization," *Int. J. Comput. Vis.*, vol. 128, no. 2, pp. 336–359, 2020.
- [8] K. Zhang, Q. Sun, C. Zhao, and Y. Tang, "Causal reasoning in typical computer vision tasks," *arXiv preprint arXiv:2307.13992*, 2023.
- [9] H. Li, Y. Liu, H. Zhang, and B. Li, "Mitigating and evaluating static bias of action representations in the background and the foreground," in *Proc. IEEE/CVF Int. Conf. Comput. Vis.*, 2023, pp. 19 854–19 866.
- [10] S. Ding, M. Li, T. Yang, R. Qian, H. Xu, Q. Chen, J. Wang, and H. Xiong, "Motion-aware contrastive video representation learning via foreground-background merging," in *Proc. IEEE/CVF Conf. Comput. Vis. Pattern Recognit.*, 2022, pp. 9706–9716.
- [11] J. Pearl, "Causal inference," in *Adv. Neural Inf. Process. Syst. Workshop*, 2010, pp. 39–58.
- [12] D. Weinland, M. Özuysal, and P. Fua, "Making action recognition robust to occlusions and viewpoint changes," in *Proc. Eur. Conf. Comput. Vis.*, 2010, pp. 635–648.
- [13] W. Liu, X. Zhong, Z. Zhou, K. Jiang, Z. Wang, and C. Lin, "Dual-recommendation disentanglement network for view fuzz in action recognition," *IEEE Trans. Image Process.*, vol. 32, pp. 2719–2733, 2023.
- [14] W. Shi, D. Li, Y. Wen, and W. Yang, "Occlusion-aware graph neural networks for skeleton action recognition," *IEEE Trans. Ind. Informatics*, vol. 19, no. 10, pp. 10 288–10 298, 2023.
- [15] Y. Chen, K. Peng, A. Roitberg, D. Schneider, J. Zhang, J. Zheng, R. Liu, Y. Chen, K. Yang, and R. Stiefelhagen, "Unveiling the hidden realm: Self-supervised skeleton-based action recognition in occluded environments," *arXiv preprint arXiv:2309.12029*, 2023.
- [16] W. Liu, X. Jia, X. Zhong, K. Jiang, X. Yu, and M. Ye, "Dynamic and static mutual fitting for action recognition," *Pattern Recognit.*, vol. 157, p. 110948, 2025.
- [17] Y. Wu, H. Qiu, J. Wen, and R. Feng, "OSD: an occlusion skeleton dataset for action recognition," in *Proc. IEEE Int. Conf. Big Data*, 2020, pp. 3355–3360.
- [18] D. Yang, K. Jiang, D. Zhao, C. Yu, Z. Cao, S. Xie, Z. Xiao, X. Jiao, S. Wang, and K. Zhang, "Intelligent and connected vehicles: Current status and future perspectives," *Sci. China Tech. Sci.*, vol. 61, pp. 1446–1471, 2018.
- [19] Z. Xie, Q. Zhang, Z. Jiang, and H. Liu, "Robot learning from demonstration for path planning: A review," *Sci. China Tech. Sci.*, vol. 63, no. 8, pp. 1325–1334, 2020.
- [20] G. Xu, T. D. Duong, Q. Li, S. Liu, and X. Wang, "Causality learning: A new perspective for interpretable machine learning," *CoRR*, vol. abs/2006.16789, 2020.
- [21] D. Xu, Y. Wu, S. Yuan, L. Zhang, and X. Wu, "Achieving causal fairness through generative adversarial networks," in *Proc. Int. Joint Conf. Artif. Intell.*, S. Kraus, Ed., 2019, pp. 1452–1458.
- [22] J. Zhang and E. Bareinboim, "Fairness in decision-making - the causal explanation formula," in *Proc. AAAI Conf. Artif. Intell.*, 2018, pp. 2037–2045.
- [23] S. Zhu, I. Ng, and Z. Chen, "Causal discovery with reinforcement learning," in *Proc. Int. Conf. Learn. Represent.*, 2020.
- [24] P. Madumal, T. Miller, L. Sonenberg, and F. Vetere, "Explainable reinforcement learning through a causal lens," in *Proc. AAAI Conf. Artif. Intell.*, 2020, pp. 2493–2500.
- [25] P. Sun, B. Wu, X. Li, W. Li, L. Duan, and C. Gan, "Counterfactual debiasing inference for compositional action recognition," in *Proc. ACM Int. Conf. Multimedia*, 2021, pp. 3220–3228.
- [26] Y. Niu, K. Tang, H. Zhang, Z. Lu, X. Hua, and J. Wen, "Counterfactual VQA: A cause-effect look at language bias," in *Proc. IEEE/CVF Conf. Comput. Vis. Pattern Recognit.*, 2021, pp. 12 700–12 710.
- [27] G. Zhou, Y. Yan, X. Zou, K. Wang, A. Liu, and X. Hu, "Mitigating modality prior-induced hallucinations in multimodal large language models via deciphering attention causality," in *The Thirteenth International Conference on Learning Representations*, 2025.
- [28] G. Jocher, A. Stoken, J. Borovec, L. Changyu, A. Hogan, L. Diaconu, F. Ingham, J. Poznanski, J. Fang, L. Yu *et al.*, "ultralytics/yolov5: v3.1-bug fixes and performance improvements," *Zenodo*, 2020.
- [29] W. Sultani, C. Chen, and M. Shah, "Real-world anomaly detection in surveillance videos," in *Proc. IEEE/CVF Conf. Comput. Vis. Pattern Recognit.*, 2018, pp. 6479–6488.
- [30] T. Lin, M. Maire, S. J. Belongie, J. Hays, P. Perona, D. Ramanan, P. Dollár, and C. L. Zitnick, "Microsoft COCO: common objects in context," in *Proc. Eur. Conf. Comput. Vis.*, 2014, pp. 740–755.
- [31] S. Liu, Z. Zeng, T. Ren, F. Li, H. Zhang, J. Yang, C. Li, J. Yang, H. Su, J. Zhu, and L. Zhang, "Grounding DINO: marrying DINO with grounded pre-training for open-set object detection," in *Proc. Eur. Conf. Comput. Vis.*, 2024.
- [32] T. Ren, S. Liu, A. Zeng, J. Lin, K. Li, H. Cao, J. Chen, X. Huang, Y. Chen, F. Yan, Z. Zeng, H. Zhang, F. Li, J. Yang, H. Li, Q. Jiang, and L. Zhang, "Grounded SAM: assembling open-world models for diverse visual tasks," *arXiv preprint arXiv:2401.14159*, 2024.
- [33] Y. Cheng, L. Li, Y. Xu, X. Li, Z. Yang, W. Wang, and Y. Yang, "Segment and track anything," *arXiv preprint arXiv:2305.06558*, 2023.
- [34] A. Kirillov, E. Mintun, N. Ravi, H. Mao, C. Rolland, L. Gustafson, T. Xiao, S. Whitehead, A. C. Berg, W. Lo, P. Dollár, and R. B. Girshick, "Segment anything," in *Proc. IEEE/CVF Int. Conf. Comput. Vis.*, 2023, pp. 3992–4003.
- [35] H. Cai, C. Gan, and S. Han, "Efficientvit: Enhanced linear attention for high-resolution low-computation visual recognition," *arXiv preprint arXiv:2205.14756*, 2022.
- [36] J. Carreira and A. Zisserman, "Quo vadis, action recognition? A new model and the kinetics dataset," in *Proc. IEEE/CVF Conf. Comput. Vis. Pattern Recognit.*, 2017, pp. 4724–4733.
- [37] C. Feichtenhofer, "X3D: expanding architectures for efficient video recognition," in *Proc. IEEE/CVF Conf. Comput. Vis. Pattern Recognit.*, 2020, pp. 200–210.
- [38] Y. Li, C. Wu, H. Fan, K. Mangalam, B. Xiong, J. Malik, and C. Feichtenhofer, "Mvitv2: Improved multiscale vision transformers for classification and detection," in *Proc. IEEE/CVF Conf. Comput. Vis. Pattern Recognit.*, 2022, pp. 4794–4804.
- [39] Z. Tong, Y. Song, J. Wang, and L. Wang, "Videomae: Masked autoencoders are data-efficient learners for self-supervised video pre-training," in *Adv. Neural Inf. Process. Syst.*, 2022.
- [40] K. Li, Y. Wang, Y. He, Y. Li, Y. Wang, L. Wang, and Y. Qiao, "Uniformerv2: Unlocking the potential of image vits for video understanding," in *Proc. IEEE/CVF Int. Conf. Comput. Vis.*, 2023, pp. 1632–1643.

- [41] L. Wang, B. Huang, Z. Zhao, Z. Tong, Y. He, Y. Wang, Y. Wang, and Y. Qiao, "Videomae V2: scaling video masked autoencoders with dual masking," in *Proc. IEEE/CVF Conf. Comput. Vis. Pattern Recognit.*, 2023, pp. 14 549–14 560.
- [42] K. Li, X. Li, Y. Wang, Y. He, Y. Wang, L. Wang, and Y. Qiao, "Videomamba: State space model for efficient video understanding," in *Proc. Eur. Conf. Comput. Vis.*, 2024.
- [43] Y. Wang, K. Li, X. Li, J. Yu, Y. He, G. Chen, B. Pei, R. Zheng, J. Xu, Z. Wang, Y. Shi, T. Jiang, S. Li, H. Zhang, Y. Huang, Y. Qiao, Y. Wang, and L. Wang, "Internvideo2: Scaling video foundation models for multimodal video understanding," *arXiv preprint arXiv:2403.15377*, 2024.
- [44] M. Contributors, "Openmmlab's next generation video understanding toolbox and benchmark," 2020.
- [45] D. Damen, H. Doughty, G. M. Farinella, S. Fidler, A. Furnari, E. Kazakos, D. Moltisanti, J. Munro, T. Perrett, W. Price, and M. Wray, "Scaling egocentric vision: The EPIC-KITCHENS dataset," in *Proc. Eur. Conf. Comput. Vis.*, 2018.